Peter J. Mikulecky
Andrew L. Feig
Department of Chemistry,
Indiana University,
800 East Kirkwood Avenue
Bloomington, IN 47401

Heat Capacity Changes Associated with Nucleic Acid Folding

Received 18 August 2005;
revised 2 November 2005;
accepted 4 January 2006
Published online 20 January 2006 in Wiley InterScience (www.interscience.wiley.com). DOI 10.1002/bip.20457

Abstract: *Whereas heat capacity changes (ΔC_Ps) associated with folding transitions are commonplace in the literature of protein folding, they have long been considered a minor energetic contributor in nucleic acid folding. Recent advances in the understanding of nucleic acid folding and improved technology for measuring the energetics of folding transitions have allowed a greater experimental window for measuring these effects. We present in this review a survey of current literature that confronts the issue of ΔC_Ps associated with nucleic acid folding transitions. This work helps to gather the molecular insights that can be gleaned from analysis of ΔC_Ps and points toward the challenges that will need to be overcome if the energetic contribution of ΔC_P terms are to be put to use in improving free energy calculations for nucleic acid structure prediction.* © 2006 Wiley Periodicals, Inc. Biopolymers 81: 38–58, 2006

This article was originally published online as an accepted preprint. The "Published Online" date corresponds to the preprint version. You can request a copy of the preprint by emailing the Biopolymers editorial office at biopolymers@wiley.com

Keywords: *nucleic acids; RNA; DNA; heat capacity change; folding; thermodynamics*

INTRODUCTION

Changes in nucleic acid structures are associated not only with changes in free energy (ΔG), enthalpy (ΔH), and entropy (ΔS), but also with significant changes in the heat capacity (ΔC_P). As will be shown, the partial molar ΔC_Ps can be large enough to affect the overall energetics of folding. Furthermore, the sign and magnitude of the partial molar ΔC_P may provide information about the molecular details of the folding process, especially with regard to the nature of the unfolded ensemble of states. This review will survey the ΔC_Ps previously reported for nucleic acid structural changes. In addition, we aim to summarize current thinking about the physical basis of ΔC_Ps associated with nucleic acid folding, the impact of ΔC_Ps on the stability of nucleic acid structures, the techniques used to measure ΔC_Ps, and finally, to point to the challenges that lie ahead.

THEORETICAL UNDERSTANDING OF HEAT CAPACITY

Heat capacity, C_P, is defined as the amount of heat required to raise the temperature of a substance by a unit degree:

$$C_P = \left[\frac{\partial q}{\partial T}\right]_P \tag{1}$$

Heat capacity is related to all other fundamental thermodynamic parameters. Consequently, various expressions relating C_P to these other parameters may be

Correspondence to: A. L. Feig; e-mail: afeig@indiana.edu

chosen as a function of experimental convenience or to emphasize some physical aspect of the system. For example, the most commonly employed relationships of C_P are

$$C_P = \left[\frac{\partial H}{\partial T}\right]_P = \left[T\frac{\partial S}{\partial T}\right]_P \quad (2)$$

Therefore, C_P can be measured as the temperature dependence of the enthalpy or entropy. Changes in C_P, such as the partial molar heat capacity associated with the folding or unfolding of a biopolymer, propagate through the expression such that

$$\Delta C_P = \left[\frac{\partial \Delta H}{\partial T}\right]_P = \left[T\frac{\partial \Delta S}{\partial T}\right]_P \quad (3)$$

Equation (3) demonstrates the most common experimental method for determining ΔC_P, by measuring ΔH as a function of temperature. The same equation also implies that ΔH and ΔS for a given transition change together and in the same direction as a function of the ΔC_P. In other words, simply by inspecting the equation, we know to expect that transitions with large ΔC_Ps should exhibit significant enthalpy–entropy compensation.[1,2]

In addition to describing ΔC_P with respect to ΔH and ΔS, we may also do so with respect to ΔG:

$$\Delta C_P = \left[-T\frac{\partial^2 \Delta G}{\partial T^2}\right]_P \quad (4)$$

ΔC_P is the second derivative of ΔG with respect to temperature. Thus, folding transitions associated with large ΔC_P values should exhibit significant curvature in a plot of ΔG versus temperature. The implications of this phenomenon will be discussed below. Experimentally, we see that in principle one can calculate the ΔC_P from a series of measurements of ΔG across a range of temperatures; in practice this task proves challenging, since uncertainty or noise in measurements of ΔG becomes more pronounced by taking the second derivative.

Finally, one can express heat capacity as the mean squared fluctuation in enthalpy or entropy at equilibrium:

$$C_P = \left[\frac{\langle \partial H^2 \rangle}{kT^2}\right]_P = \left[\frac{\langle \partial S^2 \rangle}{k}\right]_P \quad (5)$$

In addition to reinforcing the connection of C_P with enthalpy–entropy compensation, these expressions underscore a physical picture of C_P arising from the extent of energetic fluctuation within a system.[3] This concept makes sense since molecular motions essentially serve as bins in which energy is stored, such that the system resists change in temperature as heat is added to it. The concept that heat capacities are related to molecular motions in systems comprised of many weak interactions is central to some recent computational approaches to modeling heat capacity effects, as discussed below. However, whereas enthalpic/entropic fluctuations may constitute a large fraction of the total heat capacity of the system, changes in the partial molar heat capacity of solvated nucleic acids due to folding arise mostly from temperature-dependent coupled equilibria, as will be discussed.

PHYSICAL ORIGINS OF HEAT CAPACITY CHANGES IN BIOPOLYMER SYSTEMS

The partial molar heat capacity of a nucleic acid in solution derives from a combination of solvent interactions (both solute–solvent and solvent–solvent) and internal solute effects, such as conformational entropy, interconversion within ensembles of coupled states, electrostatics, vibrational modes, and others.[4] Based on decades of work on ΔC_P in protein folding, the prevailing view has been that solvent effects dominate changes in the partial molar C_P.[4–7] This perception has likely been reinforced by the fact that differential solvation of polar and nonpolar surfaces is much easier to probe experimentally than internal solute effects. Although the fundamental contributions to ΔC_P for nucleic acid folding should be the same as with other biopolymers, the balance of these factors may be different for nucleic acids,[8,9] especially given the highly polyanionic nature of DNA and RNA. Nevertheless, it is certainly the case that, when considering nucleic acid folding thermodynamics, the "system" comprises both the biopolymer and its solvation shell. For all these reasons, our summary of theory on the physical origin of ΔC_Ps in nucleic acid folding commences with a discussion of the theory describing such hydration effects. We discuss a variety of models for the interaction of water with polar and nonpolar surfaces. In addition, we consider recent work that shows how significant ΔC_Ps are a natural consequence of transitions within systems of many weak, noncovalent interactions. Finally, we describe the major impact temperature-dependent structural equilibria of single-stranded species can have on the partial molar ΔC_Ps observed for folding transitions.

Hydration of Polar and Nonpolar Surfaces

Empirical Solvent Accessible Surface Area Techniques. Early explanations of the large ΔC_Ps associated with protein folding correlated them with the hydrophobic effect.[10,11] Transfer of a nonpolar solute into water is usually accompanied by a large and positive change in C_P.[12–14] Given that protein unfolding typically exposes nonpolar (and aromatic) surfaces to solvent, it was reasoned that unfolding should also be accompanied by a large and positive ΔC_P, as is usually observed. Consequently, the most influential models for calculating folding ΔC_Ps have employed empirical data for solute transfer into water, applying these data to calculations of solvent accessible surface area (SASA) in folded versus unfolded states (reviewed in Robertson and Murphy[15]). This approach has often been effective at predicting approximate ΔC_Ps for structural transitions and still enjoys widespread use.

The SASA approach has two major elements. First, it requires a dataset describing the C_P effects of exposing polar or nonpolar surface area to solvent. These datasets typically are comprised of measurements made with small molecule model compounds, peptides, and some proteins. Phenomenologically, it turns out that, at lower temperatures (e.g., room temperature), exposing polar surface area typically decreases heat capacity whereas nonpolar exposure increases heat capacity. These trends themselves are temperature dependent, diminishing in magnitude as temperature increases.[12,13] From the model compound datasets, one calculates "area coefficients" that represent C_P per unit area of polar or nonpolar surface exposed to solvent. Different datasets vary significantly in the magnitude of the calculated area coefficients, however.[7,15] The second element of the SASA approach applies these area coefficients to solvent accessible surface areas calculated for the folded and unfolded states of a given molecule, implicitly assuming additivity of solvation effects. Calculations for the folded state can be made with confidence when they derive from crystallographic or NMR-based structures (see Figure 1). Modeling the unfolded state is far more difficult, as there is comparatively little data on the structure and heterogeneity of unfolded species.

Each of the two major elements that underlie SASA techniques is the object of criticism. First, the unique predictive capacity of any given set of area coefficients is called into question by the fact that widely varying coefficient sets can equivalently fit experimental ΔC_P data.[15] Second, the difficulty of modeling the unfolded state[18] effectively means that one can significantly alter a calculated ΔC_P simply by changing the model.

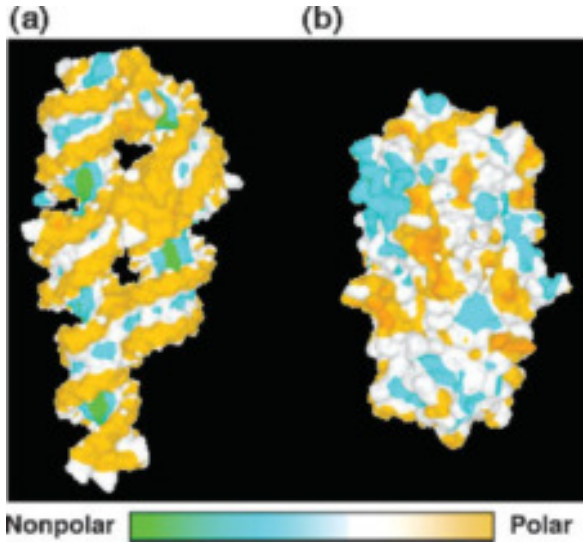

FIGURE 1 Solvent accessible surfaces for representative RNA and protein structures. Surfaces were generated with a 1.2 Å probe and colored for absolute polarity. (a) The 54-kD P4-P6 domain from the *Tetrahymena thermophila* Group I intron (PDB entry 1GID).[16] Polar and nonpolar surfaces are regularly ordered, corresponding to the phosphate backbone and grooves of RNA duplex regions. Accessible pores are visible at the center of the structure, where helices pack. (b) The 53-kD bovine lens aminopeptidase (PDB entry 1BLL).[17] Polar and nonpolar surfaces are distributed across the surface of the protein in a mosaic pattern. The protein is densely packed, with no pores extending entirely through the globular structure.

As will be shown, temperature dependence of the single-stranded state of nucleic acids can in fact be the major contributor to large ΔC_Ps measured for nucleic acid folding transitions. Nevertheless, for proteins, SASA approaches have been largely successful. Although the success of SASA approaches are often interpreted as implying a dominant role for hydration in protein ΔC_Ps, it remains possible that other effects that scale with surface area also contribute significantly.

Importantly, area coefficients that work for calculating protein ΔC_Ps do not always succeed when applied to protein–nucleic acid binding. Madan and Sharp[9] calculated the hydration ΔC_P of a series of nucleic acid constituents by using simulations with explicitly modeled water, finding that the ΔC_P associated with exposing nucleic acid polar surfaces to solvent is significantly more positive than those calculated and observed for proteins. Further, it was shown that not all polar atoms interact similarly with solvent. At a minimum, then, a SASA approach relying on a simple polar/nonpolar distinction most likely averages out important differences in the hydration of

various subgroups. In addition, the balance of hydration and other effects may differ between nucleic acids and proteins. For example, other work by Gallagher and Sharp[8] showed that long-range electrostatic effects can contribute to partial molar ΔC_P for folding transitions. Such effects, while small in protein systems, could be more pronounced during large-scale nucleic acid folding events and may be coupled to effects relating to counterion condensation.

Finally, the highly ordered arrangement of polar and nonpolar surfaces in nucleic acid structures may invalidate the assumption that solvation effects are additive.[19] Double helical secondary structures produce ordered and extensive "spines" of polar surface and grooves of nonpolar surface (Figure 1a), whereas globular proteins tend to exhibit a far less ordered distribution of polar and nonpolar surfaces (Figure 1b). Tertiary packing is also less dense in nucleic acid structures, as evidenced by the central, solvent-exposed channels apparent in the RNA structure shown in Figure 1a. Nucleic acid structures therefore have solvation properties very different from those of proteins. These differences mean that SASA methods used successfully with proteins may not transfer directly to calculations of partial molar ΔC_Ps of nucleic acid structural transitions. For example, waters solvating nucleic acid structures may behave differently from those that solvate proteins, due to interactions with the large number of condensed counterions localized in nucleic acid solvation shells. Whereas the ionic contribution to nucleic acid folding ΔC_Ps should prove to be an interesting area for study, at present the volume and quality of data specifically probing this issue are limited. In particular, much of the currently available data do not enable one to separate "pure" ionic effects on the ΔC_P from those that are actually solvent effects (i.e., deriving from exposure of bases to solvent water) linked to ionic strength-dependent changes in single-strand structure.

Qualitatively, we may expect that net hydration contributions to the ΔC_P for duplex association from stacked single strands (i.e., "docking") are small compared to those relevant to protein folding.[20] Whereas a disproportionate amount of hydrophobic surface area is buried during the folding of a typical protein, duplex association occludes from solvent a considerable amount of polar surface area (e.g., on the Watson–Crick face of paired bases); this phenomenon opposes the contribution to ΔC_P from burial of aromatic surfaces upon strand association.

Models of Water Structure. There is a vast literature devoted to the attempt to create a model of water that is computationally tractable and yet reproduces water's curious macroscopic properties (reviewed in Dill et al.[21]). Among the properties to be captured are thermal expansion, isothermal compressibility, and, importantly, heat capacity. In addition to simulating these properties for bulk water, considerable effort has been devoted to modeling aqueous solvation of both polar and nonpolar solutes. Whereas empirical SASA techniques are still the practical default for calculating ΔC_Ps associated with large-scale structural changes in biopolymers, theoretical models of solvation promise to illuminate the microscopic interactions that underlie hydration ΔC_Ps. Given the fact that hydration changes are likely to be a major factor in the partial molar ΔC_Ps associated with nucleic acid folding transitions, the ability to accurately model them would represent a major achievement in understanding the physical basis for heat capacity changes. Here, we summarize those models that most directly address C_P effects. Whether they are essentially qualitative or based on thermodynamic or statistical mechanical descriptions of solvent, all the models recapitulate the idea that water in the immediate vicinity of a biopolymer—the "solvation shell"—behaves quite differently from water in the bulk phase. These solvation shells change dramatically during macromolecular folding.

The "Iceberg" Model. More than sixty years ago, Frank and Evans[22] accounted for the positive ΔC_P associated with hydration of nonpolar solutes with the "iceberg" model, which endures as an intuitively appealing conceptual description. The model states that water molecules in the first solvation shell of a nonpolar solute are highly structured, as in ice (Figure 2a). These ice-like or clathrate structures are stabilized by favorable (negative) enthalpy that overcomes the unfavorable (negative) entropy of solvent ordering. As temperature increases, the ice-like waters "melts," gaining entropy. Concomitant with the entropic gain is a gain in enthalpy, as water–water hydrogen bonds are broken. This simultaneous rise in temperature, enthalpy, and entropy produces the observed positive ΔC_P, as expressed by Eq. (3). Greater fluctuation of the solvating waters between states is also consistent with a positive change in C_P as defined in Eq. (5). The iceberg model, however, cannot explain the negative ΔC_Ps usually observed for hydration of polar solutes, wherein solvating waters also become structured.[3,23,24] Furthermore, it has been shown that the degree of structure in water of the solvation shell cannot be as great as that observed in ice.[25] Perhaps the most important behavior suggested by the iceberg model is that water assumes distinct structural preferences as a function of both temperature and hydration of solute. More recent models attempt to describe

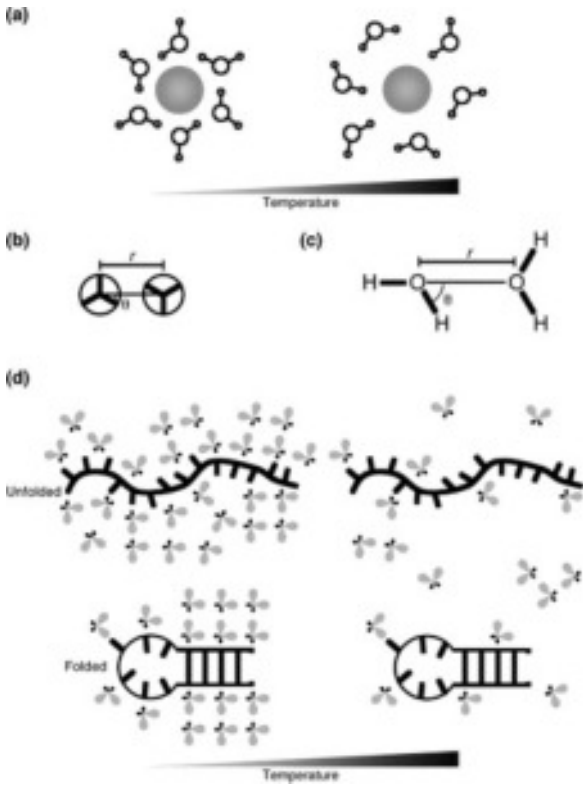

FIGURE 2 Models for hydrophobic solvation. (a) The "iceberg" model. Solvating waters form ice-like networks of favorable enthalpy. As temperature increases, these networks are disrupted and enthalpy increases. (b) The Mercedes-Benz model, adapted from Dill et al.[21] Water is modeled as a 2D disc with radial arms capable of H-bonding. Water–water interactions are described via interradial distance, r, and bonding angle, θ. Lennard–Jones and H-bonding potentials are applied as a function of r and θ. (c) The random network model, adapted from Sharp and Madan.[3] Water–water interactions are described via inter-oxygen distance, r, and angle, θ. These parameters are used to calculate mean and standard deviation of H-bond length and the root mean square H-bond angle. (d) Model for heat capacity changes arising from phase transitions within H-bonded networks, adapted from Cooper.[44] At low temperature, solute–solute, solute–solvent, and solvent–solvent H-bonding networks are extensive. As temperature increases, solute–solute bonds are lost and are not replaced with solute–solvent bonds because bonding networks are disrupted. The net loss in H-bonding results in a temperature-dependent increase in enthalpy.

these structural preferences and their thermodynamic signatures in greater detail, more generally accounting for experimentally observed C_P effects.

Two-State Thermodynamic Models. One approach to simulating the thermodynamic effects of hydration involves "two-state water," wherein water is modeled as existing in states of low hydrogen bonding (broken) or high hydrogen bonding (unbroken). Each state is assigned thermodynamic parameters based on experimental data. There are several such related models (for example, 26–28) and recent refinements.[29–31] These models fairly reproduce the observed positive ΔC_P for hydration of nonpolar surfaces as well as the temperature dependence of that ΔC_P, but they appear to do so despite an incorrect description of the ΔH and ΔS of nonpolar solute hydration.[7]

Statistical–Mechanical Models. Some of the most detailed insights into the physical basis of hydration ΔC_Ps are coming from studies in which Monte Carlo or molecular dynamics (MD) simulations of water (in various degrees of simplification) are coupled with statistical mechanical energetic treatments. Here we will briefly discuss only those approaches that most directly address C_P effects.

Mercedes–Benz Model. Based on earlier work,[23] the Mercedes–Benz (MB) model uses a simplified, two-dimensional (2D) representation of water. Water molecules are modeled as discs with three equally spaced arms (Figure 2b) that incidentally resemble the Mercedes–Benz logo.[32] Each disc is assigned parameters for Lennard–Jones attraction/repulsion and hydrogen bonding along the axes of the radial arms. Whereas hydrogen bonding is not explicitly polar in the model, it does display angular and distance dependence. Collections of MB waters are subjected to Monte Carlo simulation, and statistics are collected describing the interactions of the modeled waters. From the fluctuations in these statistical parameters one calculates average ensemble values, such as the C_P.

MB simulations are appealing because their reduced dimensionality renders them computationally tractable. Moreover, the MB model qualitatively reproduces many of the bulk properties of water, including freezing, thermal expansion, isothermal compressibility, hydrophobic solvation, and heat capacity.[21,32,33] When nonpolar solutes are modeled along with MB water, the solvating waters become locally ordered, but in a way less pronounced than seen with MB ice.[32] The success of the MB simplified model of water suggests that water behavior emerges largely as a result of its rigid hydrogen-bonding geometry. However, the MB model, like the other models so far discussed, does not explain C_P effects associated with hydration of polar surfaces.

Other Models Using MB-like Water. More recent work has exploited the computational facility of the MB model by using 2D, MB-like waters, but altering the energetic parameters associated with each water molecule modeled. For example, one approach partitions groups of three water molecules into one of three categories: cage-like, dense, or expanded.[34–36] Each category reflects a distinct geometric arrange-

ment of waters and is assigned its own set of energetic parameters. Over the course of a simulation, water triplets may fluctuate between categories. Distributions of triplets within each category are used to populate a partition function that in turn can be used to calculate ensemble-averaged macroscopic properties (e.g., heat capacity). Other methods have applied thermodynamic perturbation and integral equation theoretical treatments to MB water.[37,38] These methods largely reproduce the results of much more computationally intensive Monte Carlo simulations. A refinement on this method imparts an explicit orientation dependence to the integral equation describing water–water interactions.[39] Although these efficient analytical methods are still being developed, they promise to yield great insight into the temperature-dependent structural preferences of solvating waters.

Random Network Model. One technique for modeling water behavior does account for the opposing signs of ΔC_P for hydration of polar and nonpolar surfaces. Building on earlier work,[40,41] Sharp and coworkers have developed a method that combines a random network model of water with Monte Carlo or all-atom MD simulations.[3,9,42,43] The random network model views water as possessing some semblance of ice-like tetrahedral hydrogen bonding structure, distorted by thermal fluctuation. This behavior can be reasonably described in terms of three parameters: mean hydrogen bond length, standard deviation of hydrogen bond length, and root mean square hydrogen bond angle (Figure 2c). The model provides equations of state for macroscopic thermodynamic quantities as a function of these three parameters. A recent study[42] applied the random network model to a series of simulations with a wide range of solutes. The waters in each simulation were described in terms of a joint distribution function that considered both the separation and relative orientation of water pairs. It turned out that water pairs in solvation shells tended to cluster into one of two categories: low angle/low separation pairs (more strongly interacting) and high angle/high separation pair (more weakly interacting). Nonpolar solutes promoted the former whereas polar solutes promoted the latter, in a manner that correlated strongly with observed ΔC_Ps of hydration for the solute molecules studied. This correlation was supported by the fact that low angle/low separation water pairs undergo larger energy fluctuations than their high angle counterparts, consistent with a positive ΔC_P for nonpolar hydration. In short, the study provided a plausible structural explanation for ΔC_Ps of hydration. Whereas both polar and nonpolar solutes engendered structure in solvating waters, the angular nature of that structure differed in a thermodynamically meaningful way.

Phase Transitions in Hydrogen-Bonded Networks

The models for ΔC_Ps of hydration discussed so far largely attribute C_P effects to differential solvation of polar and nonpolar surfaces. Another line of thought suggests that the positive ΔC_Ps typically observed for unfolding transitions could be a general feature of order–disorder transitions in systems comprised of many weak interactions.[44] This view was prompted in part by the observation that even the melting of polar organic solids is accompanied by a positive ΔC_P[45] and that the significant enthalpy–entropy compensation associated with large ΔC_Ps is widely observed in weak molecular interactions.[46,47] The theory envisions folded biomolecules as "islands" of cooperatively ordered hydrogen bonds,[45] or "surface molten solids."[48] These ordered islands exist within a bulk solution of comparatively less order. Descriptive, algebraic, and statistical mechanical lattice treatments of this model[45,49,50] all produce a picture of unfolding consistent with an increase in C_P. At low temperature, unfolding does not result in a significant net loss of hydrogen bonding because solute–solute bonding is substantially replaced by solvent–solute bonding (Figure 2d). At high temperatures, however, the hydrogen bonding network of the aqueous solvent becomes disrupted, so fewer solute–solute bonds are replaced with bonds from solvent upon unfolding. The resulting net loss in hydrogen bonding occurs with positive enthalpy. Since unfolding occurs with a progressive increase in enthalpy as temperature rises, the ΔC_P for unfolding is positive. This model argues persuasively that phase transitions within hydrogen-bonded networks can contribute to observed ΔC_Ps of unfolding when nonpolar surface is exposed to solvent; it does not transparently account for negative ΔC_Ps associated with exposure of polar surfaces, however.

Temperature-Dependent Coupled Equilibria of Single Strands

Temperature-dependent, enthalpically significant coupled equilibria of unfolded species often seem to be the primary origin of ΔC_Ps observed for nucleic acid folding transitions. The potential for linked equilibria to contribute to observed ΔC_Ps has been clearly described for the unfolding of proteins engaged in coupled ligand-binding equilibria.[7,51] Similar phenomena appear to account for observed ΔC_Ps in specific binding of proteins to single-stranded DNA.[52] The model is general and applies equally well to the dissociation of nucleic acid strands engaged in linked stacking/conformational equilibria. Single-stranded nucleic acids exhibit very large temperature-dependent changes in

stacking structure, and the coupled energetics of single-stranded ordering make large contributions to overall duplex formation,[20,53–57] an issue that has been addressed recently from the standpoint of hybridization prediction algorithms.[58,59] In fact, as mentioned above, coupled stacking/unstacking events may be the dominant source of ΔC_Ps observed for duplex association, because the surfaces buried from solvent during stacked strand docking produce little net change in polar versus nonpolar hydration, as convincingly demonstrated by the groups of Record and Privalov.[20,56] One recent study demonstrated for a series of five DNA duplexes, across a wide range of ionic strengths, that the ΔC_Ps observed by calorimetry for duplex association could be quantitatively predicted from independently measured ΔHs and fractional extents of folding of the component strands.[60]

In more complicated nucleic acid folding transitions (e.g., those of multibranch helical junctions or structured RNAs), the temperature-dependent heat capacity of single-stranded regions could therefore impact the stability of intermediate folding states. The impact of such intermediate states on the stability of a native structure can be significant. For example, one study found that RNase P RNA from a thermophilic organism achieved enhanced thermal stability by folding from a less structured intermediate state than the corresponding mesophilic RNA;[61] folding from the intermediate state occurred with a ΔC_P five times larger in the thermophilic RNA.

The problem of deconvoluting coupled equilibria in nucleic acid folding ΔC_Ps is inherently difficult. Experimentally, the best way to deal with it seems to be using both thermal scanning and isothermal techniques together,[20,60,62] to assess the extent of contributions from changes in the structure of single strands. The importance of doing so is highlighted in greater detail in a later section that describes the methods frequently used to measure ΔC_Ps associated with nucleic acid folding.

IMPACT OF HEAT CAPACITY CHANGES ON NUCLEIC ACID FOLDING

Cold Denaturation

In the absence of a ΔC_P, the free energy associated with nucleic acid unfolding is linear with temperature, as expressed by the Gibbs equation:

$$\Delta G = \Delta H - T\Delta S \tag{6}$$

However, introduction of a ΔC_P introduces curvature in the temperature-dependent stability profile, as reflected by the fact that C_P is the second derivative of G with respect to temperature. In the case of nucleic acid folding transitions it is highly likely that ΔC_P itself significantly depends on temperature. To accommodate a temperature-dependent ΔC_P, the Gibbs law can be modified:

$$\Delta G = \left(\frac{T^{\mathrm{ref}} - T}{T^{\mathrm{ref}}}\right)\Delta H^{\mathrm{ref}} + \int_{T^{\mathrm{ref}}}^{T} \Delta C_P dT - \int_{T^{\mathrm{ref}}}^{T} \Delta C_P d(\ln T) \tag{7}$$

where ΔH^{ref} is the change in enthalpy upon unfolding at an arbitrary reference temperature, T^{ref}, which is often set at the high-temperature melting midpoint (i.e., the T_{M}) for convenience. Usually, there is insufficient data to usefully describe the temperature dependence of ΔC_P. Therefore, an integrated form of the modified Gibbs law is frequently used in which ΔC_P is assumed to be constant:

$$\Delta G = \Delta H^{\mathrm{ref}} - T\Delta S^{\mathrm{ref}} + \Delta C_P[(T - T^{\mathrm{ref}}) - T\ln(T/T^{\mathrm{ref}})] \tag{8}$$

where ΔS^{ref} is the change in entropy upon unfolding at the reference temperature. Two related consequences of the temperature-dependent curvature in ΔG imparted by ΔC_P (see Figure 3) are 1) that there

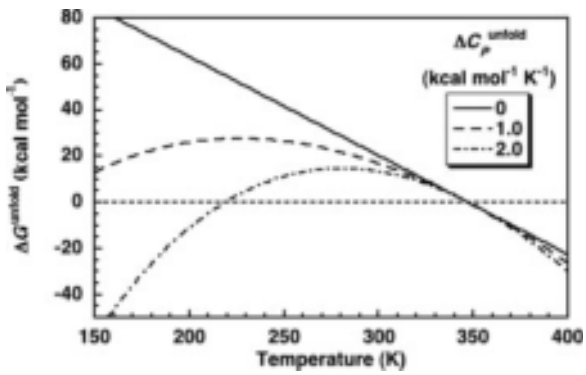

FIGURE 3 Impact of ΔC_P on structural stability. In the absence of a ΔC_P, the ΔG for unfolding is linear with temperature [Eq. (6)] and $\Delta G^{\mathrm{unfold}}$ equals zero at one point corresponding to the conventional T_{M}. The presence of a ΔC_P imparts curvature to the temperature-dependent stability of the folded state [Eq. (8)]. This curvature has two major consequences. First, there exists a temperature of maximum stability, T^{max}. Second, T^{max} is flanked by two points at which $\Delta G^{\mathrm{unfold}}$ equals zero, corresponding to both hot *and* cold melting temperatures. Stability is altered at all temperatures other than an arbitrary reference state (the high-temperature T_{M} in this plot).

exists a temperature of maximum stability, T^{max}, and 2) that unfolding can in principle be induced by sufficiently deviating in temperature either above or below T^{max}. The phenomenon of cold unfolding, or cold denaturation, has been amply demonstrated for proteins and linked to the presence of a large, positive ΔC_P for unfolding (reviewed in Privalov[63]). Due in part to the limitations of older calorimeters, it has long been assumed that ΔC_Ps were insignificant for nucleic acid folding,[64,65] although at least one early calorimetric study discussed the possibility of cold denaturation of RNA.[66] Only recently has the occurrence and impact of ΔC_Ps associated with nucleic acid folding become the focus of systematic investigation (e.g., 67–70). Attending the recent influx of ΔC_P data for nucleic acid structural changes have been further predictions of the possibility of nucleic acid cold denaturation.[67,71] Based on the magnitudes of ΔC_Ps observed for DNA and RNA oligomer duplex formation, cold denaturation transitions for such complexes would typically be expected at temperatures below –120°C.[70,71] Obviously, such temperatures are not accessible to aqueous solutions. Furthermore, the temperature dependence of nucleic acid ΔC_Ps alluded to previously makes global cold denaturation in aqueous solutions even less likely, as the ΔC_P promoting cold unfolding itself shrinks with lowered temperature due to increases in the structure of unfolded states. However, cold denaturation of RNA has been observed in solutions containing a methanol cosolvent.[72,73] In these studies of a bimolecular hammerhead ribozyme, the cosolvent permits data collection at subzero temperatures; in addition, the cosolvent destabilizes the folded state and very likely perturbs single-strand stacking equilibria in the unfolded state. An initial attempt to estimate the ΔC_P of unfolding under these conditions employed direct curve-fitting of optical melting data. This approach yielded an apparent ΔC_P for unfolding too small to account for the observed cold denaturation, possibly as a result of non-two-state folding. However, global fitting of hot and cold unfolding data across a matrix of solution conditions yielded a much larger ΔC_P that accurately predicted the observed cold melting temperature. This ΔC_P was confirmed by isothermal titration calorimetry, and it was shown that the ΔC_P was significantly methanol dependent.[73] In related work, it was shown that the catalytic domain of RNase P RNA from a thermophilic bacterium cold denatures in methanol cosolvent, but the corresponding RNA from a mesophilic bacterium does not (Takach, Mikulecky, Chen, and Feig, unpublished result). This finding was significant because the thermophilic RNA had previously been independently shown to have a fivefold larger ΔC_P than its mesophilic counterpart for unfolding to an intermediate state,[61] providing a correlation between ΔC_P and cold denaturation in those systems. It is important to recall here that the presence of cosolvent was critical to observing cold unfolding and that the molecular details of the cold-denatured state remain unclear. Given that the cosolvent concentrations used in these studies largely support hammerhead ribozyme catalysis (and therefore also support the native fold), the methanol dependence of the ΔC_P for hammerhead ribozyme unfolding probably reflects perturbations to the unfolded state. Specifically, the added methanol may have helped to preserve disorder in the single strands at low temperature, thereby helping to maintain a large ΔC_P for the folding transition. This situation recapitulates the idea that ΔC_Ps commonly observed for nucleic acid folding are intimately connected to shifts in unfolded state ensembles.

Inclusion of ΔC_P in Thermodynamic Models for Structure Prediction

Clearly, global cold denaturation of nucleic acid structure is not likely to occur in entirely aqueous solutions. Nevertheless, Eqs. (7) and (8) demonstrate that finite ΔC_Ps alter overall stability at all temperatures except T^{ref}. Widely used secondary structure prediction algorithms uniformly employ nearest-neighbors parameters that derive from van't Hoff analysis of thermal melting data wherein a zero ΔC_P is implicit.[65,74] The oligomeric duplexes used to parameterize the nearest neighbors datasets typically melt at around 50–60°C, so T^{ref} effectively lies in this range. Since temperature-dependent changes in ΔH and ΔS largely offset one another in ΔG, the zero ΔC_P approximation is usually adequate for routine stability estimations of short stretches of duplex at 37°C. The same may not be true for applications that require high-precision estimates of ΔG for hybridization of short duplexes. The temperature dependence of ΔC_P conferred by linked single-strand equilibria further complicates the prediction of folding energetics at temperatures distant from those at which parameter data are collected. One recent study directly compared two different nearest neighbors datasets, one wherein parameters were collected assuming a zero ΔC_P and the other taking ΔC_Ps into account;[69] the authors found that the extracted free energy increments differed substantially for some nearest neighbors pairs but not for others, suggesting a possible sequence dependence for ΔC_Ps of duplex formation. Such effects average out in the case of longer

duplexes, but could skew calculated stabilities of shorter ones.

Predicted values of ΔH and ΔS are less accurate than those for ΔG and vary especially between oligomeric and polymeric duplexes; inclusion of ΔC_P within stability calculations can reconcile these differences.[68,75] A more recent study by Chalikian and coworkers found that explicit consideration of ΔC_P was necessary to calculate adequate differential thermodynamic parameters ($\Delta\Delta H$, $\Delta\Delta S$) between various duplexes in an effort to understand the physical basis of their different stabilities.[70] Finally, although little is known about ΔC_Ps associated with higher order nucleic acid structures, there are some indications that they can be significant and can vary widely between structures.[61,76–78] If this emerging picture is true, then thermodynamically based three-dimensional structure prediction algorithms will need to incorporate terms for ΔC_P.

METHODS FOR MEASURING ΔC_PS ASSOCIATED WITH NUCLEIC ACID FOLDING

ΔC_Ps for nucleic acid structural changes have been obtained by many methods. Purely computational methods for calculating C_Ps associated with hydration of solvent accessible surfaces were described above. Here we summarize the major experimental approaches used to determine ΔC_P. In particular, we compare van't Hoff treatments of thermal melting data with both differential scanning calorimetry (DSC) and isothermal titration calorimetry (ITC). Finally, we highlight the ability of complementary measurements by different techniques to help deconvolute the components of ΔC_P.

van't Hoff Methods

To date, most thermodynamic measurements of nucleic acid structural changes have used van't Hoff models. Although they can be applied in several forms, all van't Hoff models essentially provide an indirect measure of ΔH —and ΔC_P —through the temperature dependence of the equilibrium constant, K, of the unfolding reaction. The models assume that molecules exist in one of two states, folded or unfolded. Any physical property that changes in proportion to the concentration of molecules in folded versus unfolded states (e.g., absorbance at 260 nm, molar ellipticity, anisotropy of a conjugated fluorophore, etc.) can be monitored to obtain K as a function of temperature. The fundamental van't Hoff relations involved are

$$\ln K = -\frac{\Delta H}{RT} + \frac{\Delta S}{R} \tag{9}$$

and the derivative of Eq. (9) with respect to temperature

$$\Delta H = -R\left(\frac{d\ln K}{d(1/T)}\right) \tag{10}$$

By taking the slope of a plot of ln K versus $1/T$, one can extract the van't Hoff ΔH for a folding transition. If a ΔC_P is associated with that transition, such a plot will exhibit curvature and the ΔH will correspond to the instantaneous slope at any given temperature. If the data density and curvature are sufficient, such plots can be fit to an expanded equation to simultaneously obtain van't Hoff values for ΔH and ΔC_P:

$$\Delta H = -R\left(\frac{d\ln K}{d(1/T)}\right) + \int_{T^{\mathrm{ref}}}^{T} \Delta C_p\, dT \tag{11}$$

This approach proves difficult, however, because noise in the measurements and the limited temperature ranges probed often conspire to mask the curvature conferred by ΔC_P.

Most frequently, bimolecular constructs are used and K is continuously perturbed by thermal scanning. The hyperchromicity at 260 nm is typically monitored as a measure of the ensemble-averaged degree of folding. If extinction coefficients are known for the folded and unfolded states—or assumed from pre- and posttransition baselines—K can be calculated from the fraction of folded molecules[79]:

$$K = \frac{\alpha}{2(1-\alpha)^2 C_{\mathrm{T}}/4} \tag{12}$$

where α is the fraction of folded molecules and C_{T} is the total strand concentration. In Eqs. (12)–(14), $C_{\mathrm{T}}/4$ is replaced by C_{T} in the case of a self-complementary duplex. The optical data can then be directly fit to yield van't Hoff values for ΔH and T_{M} by using the relation

$$K \times \frac{C_{\mathrm{T}}}{4} = \exp\left(\frac{\Delta H}{R}\left(\frac{1}{T_{\mathrm{M}}} - \frac{1}{T}\right)\right) \tag{13}$$

Since $\Delta G = 0$ at the T_{M}, ΔS can be calculated as $\Delta H/T_{\mathrm{M}}$. In principle, direct fitting models can also include ΔC_P as a fitted parameter, but the high correlation between ΔH and ΔC_P generally precludes unique solutions. Instead, one can perturb K (and thus T_{M}) simply by adjusting the total strand concentration. In this

way, one can generate a plot of ΔH versus T_M, the slope of which corresponds to the van't Hoff ΔC_P over the narrow temperature range accessible (typically $< 10^\circ$C wide).

Alternately, again exploiting the fact that $\Delta G = 0$ at the T_M, one can generate the van't Hoff expression

$$\frac{1}{T_M} = \frac{R}{\Delta H}\ln(C_T/4) + \frac{\Delta S}{\Delta H} \qquad (14)$$

By measuring T_M at a variety of strand concentrations, one can extract van't Hoff ΔH and ΔS values from the slope and intercept of a plot of $1/T_M$ versus ln (C_T/4). This approach is thought to produce more reliable values of ΔH than direct fitting[80] and has been used to generate the vast majority of data on which nearest-neighbors structure prediction algorithms rely.[74,81] Differences in ΔH values produced by these two methods are taken as an indication of non-two-state folding **or** the presence of a ΔC_P.[79] As with plots of ln K versus $1/T$, a significant ΔC_P should manifest as curvature in a plot of $1/T_M$ versus ln (C_T/4), but the same difficulties also confront attempts to fit the curvature to obtain a van't Hoff ΔC_P. For this reason, such ΔC_Ps typically require confirmation through calorimetry.

Calorimetric Methods

The use of calorimetric methods to measure the thermodynamics of nucleic acid folding transitions has increased tremendously over the last decade. This trend has been fueled by advent of high-precision microcalorimeters and by the ready availability of large amounts of chemically synthesized nucleic acids. Furthermore, the amount of high-resolution structural data for nucleic acid structures has grown dramatically, spurring interest in the physical–chemical forces that drive the formation of observed nucleic acid structures. Two calorimetric methods in particular have emerged as central, complementary tools for the direct measurement of folding thermodynamics: differential scanning calorimetry and isothermal titration calorimetry. The use of these techniques (both singly and paired) has been well-reviewed elsewhere;[82–86] we therefore do not attempt a comprehensive description of the techniques here. We address apparent differences between ΔC_Ps measured by calorimetry versus van't Hoff methods, as well as differences in ΔC_Ps obtained from thermal scanning versus isothermal calorimetry. The discussion will highlight the prominent contribution that coupled equilibria (e.g., stacking equilibria of single strands) can make to experimentally observed ΔC_Ps.

Differential Scanning Calorimetry. In a DSC experiment (Figure 4), the excess heat capacity (C_P^{XS}) of a sample solution is monitored while temperature is raised or lowered at a constant rate. Generally, this is accomplished by measuring the differential heat flow between the sample and a reference. As both sample and reference undergo temperature scanning, (un)folding reactions that occur in the nucleic acid sample will either take up or release heat, and this differential heat is obtained by subtraction of the reference thermal profile. Differential scanning calorimeters have typically operated by one of two measurement principles: heat flux or power compensation, with the latter method increasingly dominating over the last few decades for biomolecular applications. Heat flux DSC instruments employ a single heater for both sample and reference.[87] As the heater scans across temperatures, differences in heat flow that result from (un)folding events are measured by thermocouples affixed to each cell. Thus, differential heat flow results in a measurable ΔT between the two cells, from which ΔC_P is calculated. By contrast, power compensation DSC instruments measure the differential power required to maintain the sample and reference cells at equal temperature.[88] These instruments employ separate heaters for the sample and reference cells, and these heaters are controlled via feedback from coupled temperature sensors.

Folding transitions appear as peaks on thermograms from either type of instrument, and the T_M of

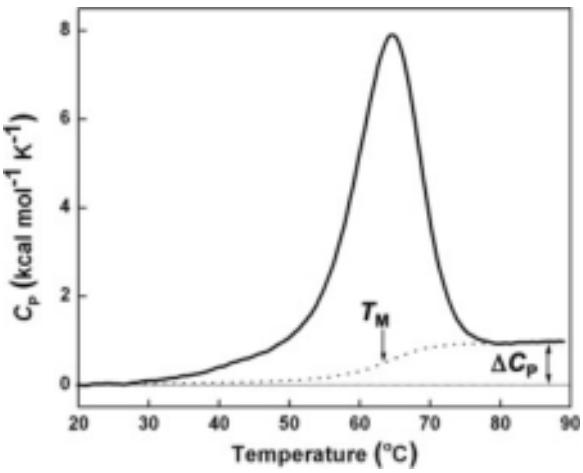

FIGURE 4 Example of DSC data for thermal melting of a 13-mer DNA duplex. The melting data (solid line) have been corrected by subtraction of a buffer blank dataset and normalized for concentration of duplex. The calorimetric ΔH for the melting transition is obtained by integrating the area under the melting peak. The data can be fit to a thermodynamic model to extract the T_M and ΔC_P, as shown. ΔC_Ps obtained from fits to DSC data incur uncertainty due to the somewhat subjective process of assigning pre- and posttransition baselines.

the transition occurs near the thermogram peak—the T_M corresponds exactly to the peak in the case of a unimolecular transition where ΔC_P equals zero. Integrating a peak with respect to temperature yields the ΔH for the transition, and the associated ΔC_P can be calculated from the difference in pre- and posttransition baselines. ΔG and ΔS can also be extracted from DSC data, but these values are indirectly obtained and are less reliable than DSC measurements of ΔH and ΔC_P. Melting data for short duplexes may require fitting to multiple transitions, to account for a premelting transition that has been attributed to fraying and/or twisting of the duplex.[56]

Peak data can be fit in ways that either accommodate finite ΔC_Ps or ignore them. The latter method yields a van't Hoff ΔH. The ratio of calorimetric to van't Hoff ΔHs can be diagnostic of intermediate folding states that occur near the T_M. Whereas DSC is in one sense ideal for determining ΔC_Ps—because it directly measures heat capacity—the method has a few drawbacks. DSC experiments can require large amounts of sample, although newer instruments can in some cases generate good data given only a few dozen micrograms. To the extent that higher concentrations must be employed relative to optical techniques (as in the case of a low-enthalpy transition), nonideal solution conditions or aggregation of denatured molecules can be problematic. For bimolecular and higher-order complexes, high sample concentrations also shift the T_M considerably upward. This phenomenon results in two problems. First, one must scan well past the transition to obtain a reliable baseline; if the T_M is too high, one either truncates the baseline or risks sample degradation that contributes to the observed heat capacity. Second, thermodynamic parameters collected by DSC apply at the T_M, and this factor is not always accounted for in reported values.[57]

The most important limit in the measurement of ΔC_Ps from DSC thermograms is that they depend heavily on the selection of pre- and posttransition baselines. Small perturbations in the regions assigned as "baseline" can produce large changes in the calculated ΔC_P. This phenomenon is further exacerbated since problems resulting from buffer mismatch between background and sample runs can lead to artifacts after baseline subtraction. Finally, in the case of RNA samples, sample degradation at high temperature can also alter the baseline, leading to additional uncertainty in these measurements. All these factors notwithstanding, DSC remains the most direct means to measure heat capacity changes associated with nucleic acid folding transitions. Continual improvements in calorimeter technology will only increase the utility of the method.

Isothermal Titration Calorimetry. During an ITC experiment (Figure 5a), small volumes of a concentrated titrant solution are injected into a titrand solution and the consequent release or absorption of heat is measured for each injection. The heat measurements are normalized against a reference cell containing a buffer blank. As with DSC instruments, most titration calorimeters used for studies of biomolecules operate by heat flux or power compensation principles, with the latter predominating for biomolecular applications. The experiment is run at a single temperature, and the differential heat flux or power required to maintain temperature in the sample and reference cells is measured and used to calculate heats of injection. Individual injection peaks are integrated to yield injection enthalpies. Plots of injection enthalpy versus the molar ratio of titrant to titrand can be fit in a model-dependent fashion to obtain ΔH, ΔS, K, and stoichiometry for the reaction. ITC is widely used to study protein–ligand binding but can also be used to investigate nucleic acid–ligand interactions or the binding and coupled folding of bimolecular nucleic acid constructs. ΔH is by far the parameter most reliably measured by ITC and, by varying the temperature, the apparent ΔC_P can be obtained without difficulty (Figure 5b). K values up to $\sim 10^9$ can usually be readily determined, and competitive binding approaches can be used to indirectly measure very tight binding.[89] ΔS is calculated from K and ΔH, and therefore incurs uncertainty from propagated error. The stoichiometry of the reaction is easily determined from the intersection of the transition midpoint with molar ratio axis of the plot. Sample requirements for ITC experiments are often less than for DSC. However, it should be noted that, in contrast to the model-free calorimetric ΔHs that can be measured in DSC experiments, enthalpy changes (and other parameters) obtained from fits to ITC data are meaningful only to the extent that the fitting model matches the experimental system. The total enthalpy change for any given titration, however, can be accurately measured regardless of how well modeled the system is.

A key feature of ITC is that, whereas parameters (ΔH and ΔS) obtained from DSC or other thermal scanning methods apply at the T_M, thermodynamic values measured by ITC relate to the temperature at which the experiment was conducted. In most cases this temperature will be significantly lower than the T_M for a given construct. As a result, "unfolded" or premixed states of nucleic acids may contain more residual structure than the same molecules at T_M. The implications of such differences in "unfolded" endstate are discussed below.

ΔC_P *Calculated by van't Hoff versus Calorimetric Methods.* Differences in ΔH (and thus ΔC_P) as measured by van't Hoff and calorimetric techniques have been the subject of intense scrutiny.[90–94] The central question is whether van't Hoff values for ΔH can be reconciled with their calorimetric counterparts by explicit inclusion of ΔC_P terms in van't Hoff analysis or whether the two methods are actually not measuring thermodynamics for exactly the same phenomena. For example, calorimetric measurements, though certainly "true," could be measuring temperature-dependent contributions of interactions with buffer components that do not show up in a van't Hoff measurement.[90] Simulations of van't Hoff data for systems exhibiting a finite ΔC_P suggested that, whereas it might not be practical to extract ΔC_P from ln K versus $1/T$ representations of equilibrium data, independently obtained ΔC_Ps could reconcile van't Hoff and calorimetric enthalpies.[92] Murphy and coworkers simulated systems wherein the equilibrium intended for study was coupled to equilibria for binding/folding[93] and protonation.[94] In each case they observed that van't Hoff and calorimetric enthalpies matched when considered over the same temperature range, provided experimental systems were allowed to fully reach equilibrium.

A central difference between van't Hoff and calorimetric determinations of ΔC_P is that van't Hoff approaches assume two-state folding transitions whereas calorimetric methods make no such assumption. This limitation of the van't Hoff model cannot be alleviated except to devise experimental means to cleanly separate folding transitions. Given the great propensity of macromolecules to participate in multistate transitions and to exhibit coupled equilibria, clean separation is often unrealized. Therefore, ITC emerges as a useful method to measure ΔH and the dependence of ΔH on temperature at physiologically relevant temperatures. Applied to nucleic acid folding, ITC has proven to be a particularly sensitive technique for measuring apparent ΔC_Ps arising from conformational equilibria of unpaired strands.

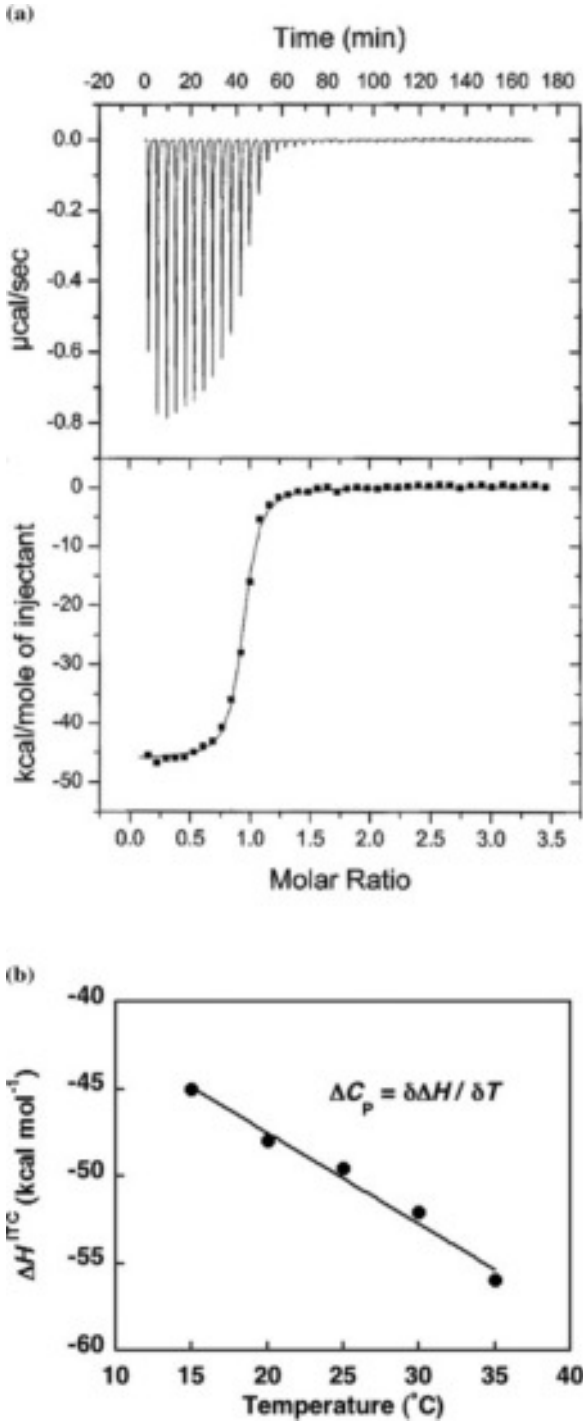

FIGURE 5 (a) Example of ITC data for the titration of a short (7-mer) RNA strand into its complement. The downward deflections in the raw thermal data (top) reflect the exothermic processes of base-pairing and coupled stacking that occur with each injection. The raw data are integrated and normalized for concentration (bottom, black squares) to produce a plot of injection enthalpy versus molar ratio (titrant : titrand). The integrated data are fit to a thermodynamic model (lower panel, solid line) to obtain the ΔH, K_A, and stoichiometry (n) for the reaction from the y-intercept, transition slope, and transition midpoint, respectively. The reaction ΔS can be calculated from the fitted ΔH and K_A. (b) ΔC_P can be determined from the temperature dependence of ΔH measured by ITC. In the figure, ΔH values obtained from ITC experiments at five temperatures are fit to a line, the slope of which corresponds to a linear approximation of the observed ΔC_P for the duplex association reaction in that temperature window (0.5 kcal mol^{-1} K^{-1} for the data shown).

Complementarity of Techniques. The mixture of techniques available to measure the thermodynamics of folding transitions includes both thermal scanning (DSC, optical melting) and isothermal (ITC) methods. These techniques measure thermodynamic parameters largely pertaining to different temperature ranges (Figure 6); the measurements may therefore correspond to different sets of thermodynamic end-states, thus complicating comparison of measured parameters from different studies. For the most part, large-scale efforts devoted to populating nearest-neighbors tables for secondary structure prediction have conscientiously employed duplexes melting within a fairly narrow temperature range,[81,95] but that range ($\sim$ 40–60°C) is significantly higher than those used in most ITC studies of nucleic acid folding. This broad range of temperatures across different types of experiment does not in itself constitute a problem, as thermodynamic parameters can be extrapolated to a common reference temperature. However, as previously emphasized, single-stranded nucleic acids can undergo enthalpically significant, temperature-dependent changes in structure. Thermal scanning studies of duplex formation therefore yield ΔH, ΔS, and ΔG values, that reflect not only the disruption of double helical duplex structure but also—at the T_M—a fairly significant progression of single helices toward a random coil-like state. By contrast, the same duplex observed by ITC at 25°C will produce thermodynamic parameters reflecting formation of the double helix from single strands that may themselves possess a large degree of stacking or other self-structure. Clearly, the end-states of the two experiments differ. Therefore, extrapolation of ΔH or ΔS to a common reference temperature by means of ΔC_P will produce different results in each case unless the ΔC_P is constant over the entire temperature range, which will only hold true for short sequences that are not prone to stacking.

For similar reasons, ΔC_Ps observed by thermal scanning methods will differ from those measured by ITC. In the former case, single strands are already significantly unfolded at the T_M, so further temperature-dependent unfolding of those strands will be relatively modest, though not absent. In contrast, perturbation of single-stranded structure across the lower temperature ranges typically sampled in ITC experiments could be very significant. In many cases, it is now clear that observed ΔC_Ps of duplex formation arise primarily from the temperature dependence of linked equilibria between structured and unstructured single strands.[20,55,56,60] Interestingly, one study that extracted ΔC_P from mechanical unfolding data for single DNA molecules revealed a temperature-dependent ΔC_P between 11 and 52°C, consistent with an increase in single-stranded structure at lower temperature.[96] Apparent ΔC_Ps involving single-stranded nucleic acids, as measured by ITC, must therefore be treated with special care; they quite possibly will not correspond to a well-defined equilibrium. On the other hand, these apparent ΔC_Ps may contain useful

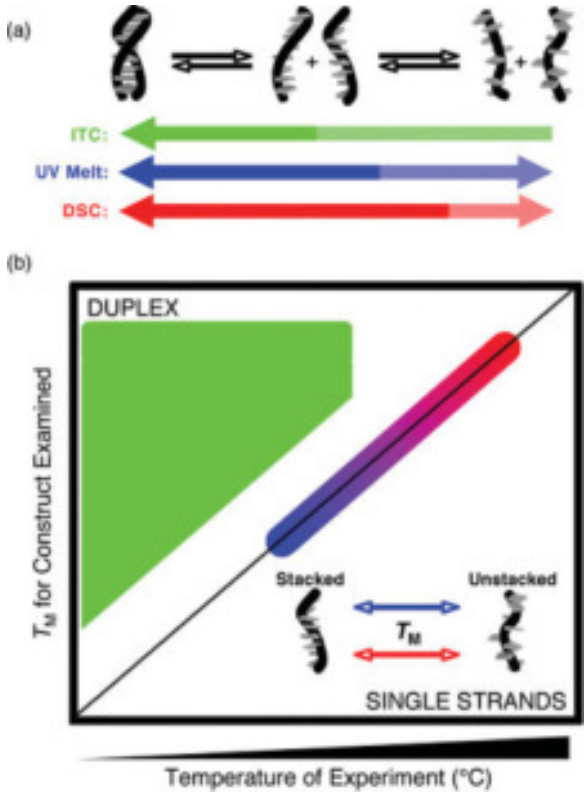

FIGURE 6 Methods for measuring ΔC_P sample different temperature ranges, where unfolded end-states may differ. (a) Schematic showing the temperature range typically probed by ITC, UV-visible melting, and DSC relative to the conformations sampled by a hypothetical duplex sample. ITC predominantly measures duplex association from partially stacked states of single strands. (b) Schematic depicting the experimental space available to ITC, UV-visible melting, and DSC with respect to the T_M of the sample. Thermal scanning techniques yield parameters relevant to the T_M, which lies within a range where single strands tend toward less-ordered states. Extrapolations of ΔH measured at T_M to lower temperature (using $\Delta C_P^{T_M}$) implicitly assume that unfolded states possess the same degree of disorder that they possess at the T_M. ITC experiments are typically conducted at lower temperatures so that duplex formation proceeds to completion; single strands may therefore proceed through many intermediate structural states. Unfolded end-states may thus be ill defined in ITC experiments performed at different temperatures (to measure ΔC_P^{ITC}), but observed ΔH^{ITC} values accurately describe reactions as they actually occur at the experimental temperatures.

thermodynamic information about single-strand equilibria. Moreover, values measured by thermal scanning methods have their own limitations. Most commonly, parameters measured from thermal scanning experiments are extrapolated to 37°C to describe the energetics of folding at physiological temperature. But these extrapolated values still implicitly reflect a transition between duplex and nearly random-coil states, an equilibrium that is probably not observed at 37°C.

SURVEY OF THE LITERATURE FOR NUCLEIC ACID FOLDING ΔC_PS

Although the literature reporting ΔC_Ps associated with nucleic acid structural changes (Table I) does not approach in scale that describing nucleic acid thermodynamics in general, reports of such ΔC_Ps nevertheless extend back several decades. Much early work involved measurements on bulk, polymeric duplex DNA, whereas more recent work has focused on shorter oligomeric DNA and RNA duplexes. Fewer studies have been attempted on nonduplex structures, but their numbers are rapidly increasing. The following survey is restricted to investigations of ΔC_Ps associated with structural changes in systems consisting only of nucleic acids; it excludes, for example, the numerous studies of ΔC_Ps observed in specific binding of nucleic acids by proteins and has similarly omitted studies of nucleic acid binding to small molecule ligands (e.g., aminoglycosides, spermine, cationic lipids, etc.).

Several trends are apparent in the values reported for polymeric nucleic acids. These values are the most consistent, often hovering near 30–60 cal mol^{-1} K^{-1} bp^{-1}. This consistency reflects both the fact that most of the reported values derive from the same technique (DSC) and that any sequence dependencies in the ΔC_P may be washed out in the case of a polymeric duplex. Despite this relative consistency, there is still noticeable variation among the values, which range from −150 to +165 cal mol^{-1} K^{-1} bp^{-1}. In several cases, widely divergent values are reported for folding transitions involving the same or very similar samples (e.g., for poly[d(AT)] · poly[d(AT)] and for genomic DNA from various organisms. There are several explanations for such inconsistencies. The most significant of these is probably the application of different approaches for estimating the ΔC_P. For example, in one study,[97] the ΔC_P associated with thermal unfolding of poly[d(AT)] · poly[d(AT)] was estimated both from pre- and posttransition baselines of DSC data (∼ 20 cal mol^{-1} K^{-1} bp^{-1}) and from the variation with temperature of DSC-measured ΔHs for the transition across a range of DNA concentrations (–150 cal mol^{-1} K^{-1} bp^{-1}).[97] The two techniques yielded dramatically different estimates for ΔC_P, clearly indicative of a problem with one or both experiments. Another study used DSC to measure ΔHs and T_Ms for poly[d(AT)] · poly[d(AT)] melting across a range of ionic strengths and concluded that there was no significant ΔC_P associated with unfolding.[98] Combined with the relative insensitivity of early calorimeters, the use of these different approaches apparently masked the actual ΔC_P, within error. More recent measurements on poly[d(AT)] · poly[d(AT)], using more advanced calorimeters, have produced ΔC_P values of 40–60 cal mol^{-1} K^{-1} bp^{-1}, within the consensus range for polymeric DNAs.[70,75] Other early investigations of genomic DNA[99,100] or poly(rA)[101] calculated ΔC_Ps by observing $\Delta H(T_M)$ as perturbed by varying pH, a practice that may introduce uncertainty from coupled heats of ionization. Finally, one study revealed a systematic discrepancy between ΔC_Ps measured by ITC versus DSC for a series of polymeric DNAs[70]; in each case, the ΔC_P measured at lower temperature by ITC was of larger magnitude than its counterpart, measured at higher temperature by DSC. This observation could point toward the temperature dependence of ΔC_P for nucleic acid transitions, unrecognized at the time, rather than a fundamental problem with one of the actual measurements.

Table I identifies 13 individual studies that reported ΔC_Ps for oligomeric duplexes. Notably, studies employing all varieties of measurement detect significant changes in heat capacity for duplex/triplex folding, although some early DSC studies failed to detect any ΔC_P from pre- and posttransition baselines.[54,102] In many of these studies multiple duplexes were analyzed, yielding ranges of values for the individual sequences involved. In the table, these values have been normalized for length and are reported per bp, but we do this with a certain amount of trepidation as it implies a uniformity that really may not be present. What is evident from these studies, especially those that compared multiple sequences side-by-side, is that there is extensive variability in the measured values ranging from slightly negative (–30 cal mol^{-1} K^{-1} bp^{-1}) to significantly positive (332 cal mol^{-1} K^{-1} bp^{-1}). Some of the variability comes from the use of multiple methodologies and hence different temperature regimes for the measurements. These short sequences, however, are much more likely to exhibit sequence-dependent effects than their long polymeric cousins described above; within these sequence dependencies most likely lies a large amount of the variability.

As described above, much, if not all, of the sequence- and ion-dependence results from issues relating to the structure of the single-stranded state. A few studies have explicitly probed for the effects of ionic

Table I Summary of Reported ΔC_PS for Nucleic Acid Structural Changes[a]

ΔC_P (cal (mol K)$^{-1}$)	Temperature (°C)	Method[b]	Ionic Conditions	Notes	Reference
Polymeric nucleic acids					
~ 15 (bp)$^{-1}$	5–40	Viscosity/calorimetry	0.1 *M* NaCl	A, B	100
~ 50 (bp)$^{-1}$	10–40	Mixing calorimetry	0.1 *M* KCl	D	108
~ 80 (bp)$^{-1}$	5–40	Mixing calorimetry	0.1 *M* NaCl	A, B	99
~ 40 (bp)$^{-1}$	$\sim$ 50–72	DSC	0.01–0.5 *M* "cation"	B, D	109
~ 30 (bp)$^{-1}$	28–68	DSC	0.01–0.26 *M* NaCl	B, D	110
~ 40 (bp)$^{-1}$	$\sim$ 70–75	DSC	0.46–0.57 *M* NaCl	B, D	111
~ 50 (bp)$^{-1}$	32–86	DSC	0.5 *M* NaCl	B, C	101
~ 20 vs. -150 (bp)$^{-1}$	39–43	DSC; baselines vs. $d\Delta H/dT_M$	0.007 Na salts	E, G	97
~ 30 (bp)$^{-1}$	64–85	DSC	0.01–0.15 *M* NaCl	A, B	64
0 vs. ~ 30 (bp)$^{-1}$	55–79	DSC, vary %GC of DNAs	0.0025 Na/K salts	A	112
40 (bp)$^{-1}$	58–77	DSC	0.001–0.05 *M* NaCl	A, B	113
65 (bp)$^{-1}$	64–100	DSC	0.01–3.2 *M* NaCl	A, B	114
165 ± 24 (bp)$^{-1}$	28	Drop calorimetry	0.1 *M* NaCl	C	115
140 ± 28 (bp)$^{-1}$	28	Drop calorimetry	0.1 *M* NaCl	D	115
30 ± 4 (bp)$^{-1}$	$\sim$ 35–60	DSC	0.01–0.1 *M* NaCl	B, D	116
~ 0	49–75	DSC	0.01–1.0 *M* NaCl	G	98
35 ± 8 (bp)$^{-1}$	50–85	DSC	0.001–0.15 *M* NaCl	A, B	103
32–37 (bp)$^{-1}$	64–103	High pressure light scattering	0.005–0.5 KCl	A, B	117
80 ± 20 (bp)$^{-1}$	42–68	DSC	0–0.04 *M* NaCl or LiCl	A, E	118
30 ± 20 (bp)$^{-1}$	45	DSC	0.03–0.2 *M* NaCl	F	75
60 ± 20 (bp)$^{-1}$	51	DSC	0.03–0.2 *M* NaCl	G	75
100 ± 30 (bp)$^{-1}$	58	DSC	0.03–0.2 *M* NaCl	H	75
40 (bp)$^{-1}$	80	DSC	0.03 *M* NaCl	I	75
78 (bp)$^{-1}$	104	DSC	0.03 *M* NaCl	J	75
20–80 (bp)$^{-1}$	$\sim$ 45–95	OM	0.001–1 *M* NaCl	A	67
30 ± 10 (bp)$^{-1}$	$\sim$ 15–60	OM	0.01–0.1 *M* NaCl	A, K, L	71
60 ± 10 (bp)$^{-1}$	11–52	Mechanical unfolding	0.5 *M* NaCl	A, M	96
50 ± 20 (bp)$^{-1}$/ 40 ± 20 (bp)$^{-1}$	25–40/ $\sim$ 40–70	ITC/DSC	$\sim$ 0.02–0.3 *M* NaCl	G	70
70 ± 20 (bp)$^{-1}$/ 40 ± 40 (bp)$^{-1}$	25–40/ $\sim$ 40–70	ITC/DSC	$\sim$ 0.02–0.3 *M* NaCl	H	70
70 ± 10 (bp)$^{-1}$/ 60 ± 60 (bp)$^{-1}$	25–40/ $\sim$ 40–70	ITC/DSC	$\sim$ 0.02–0.3 *M* NaCl	F	70
40 ± 30 (bp)$^{-1}$	$\sim$ 40–70	DSC	0.01–0.05 *M* NaCl	J, B	70
60 ± 10 (bp)$^{-1}$/ 30 ± 10 (bp)$^{-1}$	25–40/ $\sim$ 40–70	ITC/DSC	$\sim$ 0.02–0.3 *M* NaCl	B, D	70
70 ± 10 (bp)$^{-1}$/ 40 ± 20 (bp)$^{-1}$	25–40/ $\sim$ 40–70	ITC/DSC	$\sim$ 0.02–0.3 *M* NaCl	B, N	70
Oligomeric duplexes					
~ 0	46	DSC	1 *M* NaCl	O	102
96 (bp)$^{-1}$	$\sim$ 15–35	OM	1 *M* NaCl	O	79
79 (bp)$^{-1}$	$\sim$ 25–45	OM	1 *M* NaCl	P	79
71 (bp)$^{-1}$	$\sim$ 25–45	OM	1 *M* NaCl	P	79
73 (bp)$^{-1}$	$\sim$ 45–55	OM	1 *M* NaCl	O	79
53 (bp)$^{-1}$	$\sim$ 35–50	OM	1 *M* NaCl	P	79
128 ± 32 (bp)$^{-1}$	$\sim$ 40–90	DSC	0.001–2 *M* NaCl	B, Q	103
20–160 (bp)$^{-1}$	$\sim$ 15–70	OM	1 *M* NaCl	O	119
20–170 (bp)$^{-1}$	$\sim$ 5–65	OM	1 *M* NaCl	R	120
44 (bp)$^{-1}$	46	DSC	1 *M* NaCl	S	121

Table I (*Continued*)

ΔC_P (cal (mol K)$^{-1}$)	Temperature (°C)	Method[b]	Ionic Conditions	Notes	Reference
~ 0	74	DSC	1 *M* NaCl	T	54
170 (bp)$^{-1}$	35–50	ITC	0.1 *M* NaCl	T	55
93 ± 7 (bp)$^{-1}$	9–39	ITC	0.12 *M* NaCl	B, T	20
60 ± 30 (bp)$^{-1}$	66	DSC	0.12 *M* NaCl	T	20
50 ± 10 (bp)$^{-1}$	8–45	ITC and DSC	0.1 *M* KCl	T	56
7–332 (mean: 95) (bp)$^{-1}$	15–53	OM	1 *M* NaCl	T	69
35–236 (mean: 115) (bp)$^{-1}$	11–56	OM	1 *M* NaCl	U	69
−30 to +20 (bp)$^{-1}$	5–20	ITC	0.1–1 *M* NaCl	V	62
+10 to +60 (bp)$^{-1}$	5–20	ITC	0.1–1.5 *M* NaCl	V	62
60–120 (bp)$^{-1}$	15–45	ITC	0.1–1 *M* NaCl	T	60
Hairpins					
800–1530	$\sim$ 5–40	ln *K* vs. 1/*T*	0.1 *M* NaCl	W, X	122
390–1060	$\sim$ 5–40	ln *K* vs. 1/*T*	0.5 *M* NaCl	W, X	122
410–1470	$\sim$ 60–90	DSC	0.1 *M* NaCl	Y	123
75 ± 30 (bp)$^{-1}$	$\sim$ 45–75	DSC	0.1 *M* NaCl	Z	124
50–130 (CAG)$^{-1}$	54–59	OM and DSC	$\sim$ 0.01–0.5 *M* KCl	Y	125
Triplexes					
90 ± 11 (base triple)$^{-1}$	12–37	DSC	2.6–3.7 *M* NaCl	AA	126
914 ± 47 (61 (base triple)$^{-1}$)	15–35	ITC	0.2 *M* NaCl, 20 m*M* $MgCl_2$	BB	127
600 (55 (base triple)$^{-1}$)	10–35	ITC	0.3 *M* NaCl	CC	128
1200 (55 (base triple)$^{-1}$)	15–35	ITC	0.02 *M* $MgCl_2$	DD	129
16 ± 1 (base triple)$^{-1}$	29–62	DSC	0.17–0.6 *M* NaCl	B, EE	130
53 ± 6 (base triple)$^{-1}$	40–74	DSC	0.17–0.62 *M* NaCl	B, FF	130
52 ± 4 (base triple)$^{-1}$	38–70	DSC	0.25–0.75 *M* NaCl	B, GG	130
Helical junctions					
970 ± 50	12–30	ITC	0.2 *M* NaCl, 0.01 *M* $MgCl_2$	HH	131
1600 ± 200	10–25	ITC	0.01 *M* NaCl, 5 m*M* $MgCl_2$	II	132
2800	37–83	DSC	0.1 *M* KCl, 2 m*M* $MgSO_4$	JJ	133
3600	4–75	ln *K* vs. 1/*T* FRET	1 m*M* $MgCl_2$	KK, LL	104
3900	4–75	ln *K* vs. 1/*T* FRET	1 m*M* $MgCl_2$	KK, MM	104
1700	4–75	ln *K* vs. 1/*T* FRET	1 m*M* $MgCl_2$	KK, NN	104
−2400 and 300–2000	$\sim$ 15–50	OM	1 *M* NaCl	JJ	76
−670 to 780	10–25	ITC	0.1 *M* NaCl, 0–15 m*M* $MgCl_2$	JJ	134
800 ± 200	−1 to 53	OM	0.5 *M* NaCl	JJ, OO, PP	72
300–5000 (average 1700)	$\sim$ 45–55	OM	1 *M* NaCl	JJ	77
−200 to 3600 (average 1700)	$\sim$ 45–55	OM	1 *M* NaCl	NN	77
3400 ± 300	−18 to 60	OM	0.5 *M* NaCl	JJ, OO, PP	73
1000–2900	25–40	ITC	0.5 *M* NaCl	JJ, PP	73
900 (net); 1400 (helices); 500 (core); ± 100 for all	5–35	ITC	1 *M* NaCl or 10 m*M* $MgCl_2$	JJ	78
Higher order structures					
3000	$\sim$ 30–70	OM and batch calorimetry	0.005 *M* NaCl, 0–1 m*M* $MgCl_2$	B, RR	66, 135
~ 0	49–79	DSC and batch calorimetry	0–1 *M* NaCl, 1–80 m*M* $MgSO_4$	B, RR	106
1200–7000	67–81	DSC	0.05–5 m*M* $MgCl_2$	B, RR	105

Table I (*Continued*)

ΔC_P (cal (mol K)$^{-1}$)	Temperature (°C)	Method[b]	Ionic Conditions	Notes	Reference
~ 0	$\sim$ 40–80	DSC	0.02–0.15 *M* NaCl, 1–10 m*M* $MgCl_2$	B, RR	107
3300	52–73	DSC	0.1 *M* KCl	RR	136
155	52	DSC	0.1 *M* KH_2PO_4	QQ	137
2500 $\pm$ 300	10–70	ΔG vs. T	1 m*M* $MgCl_2$	RR	61
460 $\pm$ 120	10–70	ΔG vs. T	1 m*M* $MgCl_2$	RR	61

[a]Entries are ordered first by sample type (polymeric, oligomeric, hairpins, triplexes, helical junctions, and higher order structures) and then by year of publication.

[b]DSC, differential scanning calorimetry; ITC, isothermal titration calorimetry; OM, optical melting; FRET, Fluorescence resonance energy transfer.

A: polymeric DNA.
B: Calculated from ΔH vs. T_M, where T_M was perturbed by varying ionic/pH conditions.
C: poly(rA) · poly(rA).
D: poly(rA) · poly(rU).
E: Calculated from ΔH vs. T_M, where T_M was perturbed by varying [DNA].
F: poly[d(IC)] · poly[d(IC)].
G: poly[d(AT)] · poly[d(AT)].
H: poly[d(A)] · poly[d(T)].
I: poly[d(AC)] · poly[d(GT)].
J: poly[d(GC)] · poly[d(GC)].
K: Pressure modulation study.
L: Study also included DNA : RNA hybrids and analysis of homopolymeric RNAs.
M: Mechanical unfolding study.
N: poly(rI) · poly(rC).
O: Self-complementary RNA duplex.
P: Self-complementary RNA duplex with dangling ends.
Q: 145-bp duplex DNA.
R: Series of 8 RNA duplexes, 6- to 8-mers, with single mismatches.
S: Self-complementary DNA duplex.
T: Non-self-complementary DNA duplex.
U: DNA · RNA chimeric duplexes.
V: Non-self-complementary RNA duplex.
W: Values for dimer–monomer dissociation for palindromic sequences.
X: K_d determined by analytical ultracentrifugation.
Y: DNA hairpins with triplet-repeat composition $(XXX)_6$.
Z: DNA hairpins with tandem mismatches.
AA: polymeric $(dT)_n \cdot 2(dA)_n$ triplex.
BB: 15-mer DNA single strand titrated into 23-mer duplex DNA to form triplex.
CC: 11-mer DNA single strand titrated into 17-mer duplex DNA to form triplex.
DD: 22-mer DNA single strand titrated into 30-mer duplex DNA to form triplex.
EE: Dissociation of poly(dU) from polymeric AUU triplex.
FF: Dissociation of poly(dT) from polymeric ATT triplex.
GG: Dissociation of poly(dU) from polymeric ATU triplex.
HH: DNA 4-way junction.
II: DNA 3-way junction.
JJ: RNA 3-way junction.
KK: Hairpin ribozyme.
LL: 2-Way junction.
MM: 3-Way junction.
NN: 4-Way junction.
OO: Based on $\Delta\Delta H/\Delta T_M$ as derived from curve-fitting of hot and cold melting.
PP: Measurements in the presence of MeOH cosolvent.
QQ: DNA quadruplex.
RR: Tertiary folded RNA, either $tRNA^{Phe}$, *E. coli* α operon mRNA, or RNase P.

strength on ΔC_Ps associated with duplex folding. Whereas no significant ionic effect was observed at low salt concentrations,[20] mixed results have been obtained in investigations probing wider ranges of added salt; one DSC study did not detect any ionic effect on ΔC_P even when 2 *M* NaCl was present in solution, but ITC measurements probing the effect on ΔC_P for RNA duplex formation found a log-linear relationship up to 1.5 *M* added NaCl.[62] A follow-up examination of DNA duplex formation revealed that both added salt and sequence composition modulated ITC-detected ΔC_Ps via perturbations to single-strand stacking.[60] Thus, conditions that promote single-stranded stacking (low temperature and elevated ion concentrations) will typically exhibit extreme temperature dependence in ΔC_P. At one extreme, high salt concentrations at very low temperature will result in duplex association from stacked strands, accompanied by a small or negligible ΔC_P. As the experimental temperature range passes over the T_Ms for the component single strands (as in many ITC experiments), ΔC_Ps measured for duplex formation will reflect the coupled temperature-dependent ΔHs for single-strand stacking and will therefore be much larger. Finally, when ΔC_Ps are measured at temperatures above the T_Ms for the component single strands (as in most DSC experiments), duplexes dissociate to mostly unstacked strands; thus, the observed ΔC_P reflects exposure of unstacked bases to solvent, but largely lacks the contribution of coupled temperature-dependent equilibria. These ionic strength effects are only evident, however, for sequences and temperature regimes prone to single-stranded stacking, explaining why this phenomenon is observed in ITC studies while being absent in thermal melting experiments such as those of Chipev and Angelova.[103]

Several studies have reported ΔC_Ps for hairpin melting, particularly for branched structures formed by extended triad repeats. In these cases, the exact structure to which the measured ΔC_P applies is not always defined. Thus, the ΔC_P may be used to help gain a sense of the molecular nature of triad repeat structures, but assessing the molecular origin of the phenomenon is premature. The trends observed for duplexes will likely perpetuate through these studies, but much more work remains to be done in this area.

The most diverse set of values listed in Table I pertain to helical junction structures, where both van't Hoff and calorimetric techniques reveal a wide range of observed ΔC_Ps for junction folding. This situation likely reflects the fact that formally unpaired junction regions are prone to idiosyncratic folds and may be particularly disposed to partially structured intermediates that dramatically affect the measured ΔC_P. Much work remains to be done to unravel the molecular basis of ΔC_Ps observed in the folding of these vital and widespread motifs.

Currently, comparisons are best made within the context of studies that probed several sequences side-by-side. One such study by Klostermeier and Millar showed that a four-way junction exhibited a ΔC_P half that of its two-way and three-way counterparts, with all other aspects of the construct held constant.[104] Similarly, the Turner lab systematically analyzed approximately 20 three-helix junctions differing in the sequence context within the junction region; the junction folding ΔC_Ps varied over almost 5000 cal mol^{-1} K^{-1}.[76,77] Thus, the contribution from these junctions to the overall ΔC_P observed for a folding of a nucleic acid can be huge, potentially dwarfing the partial molar heat capacity changes from the helical elements. Variations in the observed ΔC_P may become a useful indicator of differences in junction folding, due in part to the previously discussed connection of observed ΔC_Ps with temperature-dependent heat capacity changes in single-stranded nucleic acids. Currently, however, insufficient data exist to fully understand this phenomenon.

A significant challenge in this area is the need to deconvolute and parameterize the effects that contribute to the ΔC_P for folding of a nucleic acid, since that will be the only way to incorporate these thermodynamic contributions into predictive folding algorithms. One study used the hammerhead ribozyme as a model three-way junction, successfully deconvoluting the helical and junction components of ΔC_P,[78] but this methodology has yet to be extended to a broader range of junction sequences or geometries.

Very few studies have reported ΔC_Ps for the folding of larger, structured RNAs. This scarcity of data is largely due to experimental difficulty. Structured RNAs often require the addition of divalent cations to fold in vitro, and these cations promote hydrolysis of the RNAs at the high temperatures sampled by thermal melting techniques, thus obscuring high temperature baselines. The inherent difficulty of these kinds of measurements is exemplified by the conflicting values obtained for the ΔC_P associated with folding of $tRNA^{Phe}$. Whereas two independent calorimetric determinations of the ΔC_P for $tRNA^{Phe}$ unfolding produced very large values,[66,105] a separate pair of studies on the same molecule concluded that the ΔC_P was essentially zero, within error.[106,107] According to the final of the four analyses, the large heat capacity change measured in the initial study appeared to have been an artifact of sample degradation (at high temperature in the presence of $MgCl_2$) that obscured a

posttransition baseline within DSC data.[107] ITC analysis of large RNAs typically requires either that cations be directly titrated into the RNA sample to promote folding (which results in significant heats of ion condensation coupled to folding) or that the RNA be engineered as a bimolecular construct. Finally, even a successfully measured ΔC_P presents the challenge of interpretation with respect to defined structures.

Overall, the database highlights the recent rise in reported ΔC_Ps for nucleic acid folding transitions, a growing awareness of the need to apply multiple thermodynamic techniques to study folding transitions, increased interest in measuring ΔC_Ps for structures more complicated than duplexes, and the continuing challenge of deconvoluting measured ΔC_Ps into well-defined physical phenomena. In the long term, the hierarchical nature of nucleic acid folding will likely benefit investigations of its associated ΔC_Ps. Better understanding of duplex folding ΔC_Ps will enable more detailed interpretations of ΔC_Ps observed for helical junction folding; this, in turn, will facilitate the study of large, structured RNAs through a divide-and-conquer approach.

THE ROAD AHEAD

The systematic, extensive study of ΔC_Ps associated with nucleic acid folding, a fairly recent and emerging endeavor, is being accelerated by the wide availability of sensitive equipment for making thermodynamic measurements, the decreasing expense of synthetic nucleic acids, and the explosion of high-resolution nucleic acid structural data. The field is ripe for advancement, but faces theoretical and experimental challenges.

A well-developed body of theory originally devised to describe protein ΔC_Ps is being calibrated against nucleic acids, and early results are mixed. Whereas hydration clearly plays a major role in nucleic acid ΔC_Ps, the contributions of electrostatic effects and the impact of condensed counterions on the solvation shell are poorly understood. Moreover, the precise physical origins of hydration ΔC_Ps are still a matter of debate. Statistical mechanical treatments of explicitly simulated solvation are lending insight in this area. Eventually, one unified theory of water behavior should quantitatively account for ΔC_Ps of hydration in both proteins and nucleic acids.

Calorimetric data on nucleic acid structural changes are burgeoning within the literature. This encouraging development has prompted the need to address differences in ΔC_Ps observed by different techniques, operating in different temperature windows. In particular, it will be necessary to parse from observed ΔC_Ps the sometimes dominant contribution of linked, temperature-dependent equilibria of single strands. This analysis will be critical to efforts to tie observed ΔC_Ps to specific physical phenomena. The key will be to study systems by multiple methods and integrate results to achieve the most complete thermodynamic description.

As we progress through these various challenges, theory and experiment can increasingly move into a fruitful dialectic, hopefully coalescing into a much deeper understanding of the role played by ΔC_Ps in modulating nucleic acid folding and into a general agreement about the physical properties on which they report.

REFERENCES

1. McPhail, D.; Cooper, A. J Chem Soc Farad Trans 1997, 93, 2283–2289.
2. Sharp, K. Protein Sci 2001, 10, 661–667.
3. Sharp, K. A.; Madan, B. J Phys Chem B 1997, 101, 4343–4348.
4. Sturtevant, J. M. Proc Natl Acad Sci U S A 1977, 74, 2236–2240.
5. Spolar, R. S.; Record, M. T., Jr. Science 1994, 263, 777–784.
6. Makhatadze, G. I. Biophys Chem 1998, 71, 133–156.
7. Prabhu, N. V.; Sharp, K. A. Annu Rev Phys Chem 2005, 56, 521–548.
8. Gallagher, K.; Sharp, K. Biophys J 1998, 75, 769–776.
9. Madan, B.; Sharp, K. A. Biophys J 2001, 81, 1881–1887.
10. Kauzmann, W. Adv Protein Chem 1959, 14, 1–63.
11. Dill, K. A. Biochemistry 1990, 29, 7133–7155.
12. Makhatadze, G. I.; Privalov, P. L. J Mol Biol 1990, 213, 375–384.
13. Privalov, P. L.; Makhatadze, G. I. J Mol Biol 1990, 213, 385–391.
14. Murphy, K. P.; Gill, S. J. J Mol Biol 1991, 222, 699–709.
15. Robertson, A. D.; Murphy, K. P. Chem Rev 1997, 97, 1251–1267.
16. Cate, J. H.; Gooding, A. R.; Podell, E.; Zhou, K.; Golden, B. L.; Kundrot, C. E.; Cech, T. R.; Doudna, J. A. Science 1996, 273, 1678–1685.
17. Kim, H.; Lipscomb, W. N. Biochemistry 1993, 32, 8465–8478.
18. Dill, K. A.; Shortle, D. Annu Rev Biochem 1991, 60, 795–825.
19. Chalikian, T. V.; Breslauer, K. J. Biopolymers 1998, 48, 264–280.
20. Holbrook, J. A.; Capp, M. W.; Saecker, R. M.; Record, M. T. Biochemistry 1999, 38, 8409–8422.

21. Dill, K. A.; Truskett, T. M.; Vlachy, V.; Hribar-Lee, B. Annu Rev Biophys Biomol Struct 2005, 34, 173–199.
22. Frank, H. S.; Evans, M. W. J Chem Phys 1945, 13, 507.
23. Ben-Naim, A. J Chem Phys 1971, 54, 3682–3695.
24. Marcus, Y. Biophys Chem 1994, 51, 111–127.
25. Lipscomb, L. A.; Zhou, F. X.; Williams, L. D. Biopolymers 1996, 38, 177–181.
26. Gill, S. J.; Dec, S. F.; Olofsson, G.; Wadso, I. J Phys Chem 1985, 89, 3758–3761.
27. Muller, N. Acc Chem Res 1990, 23, 23–28.
28. Lee, B.; Graziano, G. J Am Chem Soc 1996, 118, 5163–5168.
29. Silverstein, K. A. T.; Haymet, A. D. J.; Dill, K. A. J Am Chem Soc 2000, 122, 8037–8041.
30. Bakk, A.; Hoye, J. S.; Hansen, A. Biophys J 2001, 81, 710–714.
31. Bakk, A.; Hoye, J. S.; Hansen, A. Biophys J 2002, 82, 713–719.
32. Silverstein, K. A. T.; Haymet, A. D. J.; Dill, K. A. J Am Chem Soc 1998, 120, 3166–3175.
33. Southall, N. T.; Dill, K. A.; Haymet, A. D. J. J Phys Chem B 2002, 106, 521–533.
34. Truskett, T. M.; Dill, K. A. J Phys Chem B 2002, 106, 11829–11842.
35. Truskett, T. M.; Dill, K. A. J Chem Phys 2002, 117, 5101–5104.
36. Truskett, T. M.; Dill, K. A. Biophys Chem 2003, 105, 449–459.
37. Urbic, T.; Vlachy, V.; Kalyuzhnyi, Y. V.; Southall, N. T.; Dill, K. A. J Chem Phys 2000, 112, 2843–2848.
38. Urbic, T.; Vlachy, V.; Kalyuzhnyi, Y. V.; Southall, N. T.; Dill, K. A. J Chem Phys 2002, 116, 723–729.
39. Urbic, T.; Vlachy, V.; Kalyuzhnyi, Y. V.; Dill, K. A. J Chem Phys 2003, 118, 5516–5525.
40. Henn, A. R.; Kauzmann, W. J Phys Chem 1989, 93, 3770–3783.
41. Rice, S. A.; Sceats, M. G. J Phys Chem 1981, 85, 1108–1119.
42. Gallagher, K. R.; Sharp, K. A. J Am Chem Soc 2003, 125, 9853–9860.
43. Madan, B.; Sharp, K. J Phys Chem 1996, 100, 7713–7721.
44. Cooper, A. Curr Opin Chem Biol 1999, 3, 557–563.
45. Cooper, A. Biophys Chem 2000, 85, 25–39.
46. Dunitz, J. D. Chem Biol 1995, 2, 709–712.
47. Searle, M. S.; Westwell, M. S.; Williams, D. H. J Chem Soc Perkin Trans 2 1995, 141–151.
48. Zhou, Y.; Vitkup, D.; Karplus, M. J Mol Biol 1999, 285, 1371–1375.
49. Cooper, A.; Johnson, C. M.; Lakey, J. H.; Nollmann, M. Biophys Chem 2001, 93, 215–230.
50. Cooper, A. Biophys Chem 2005, 115, 89–97.
51. Eftink, M. R.; Anusiem, A. C.; Biltonen, R. L. Biochemistry 1983, 22, 3884–3896.
52. Ferrari, M. E.; Lohman, T. M. Biochemistry 1994, 33, 12896–12910.
53. Appleby, D. W.; Kallenbach, N. R. Biopolymers 1973, 12, 2093–2120.
54. Vesnaver, G.; Breslauer, K. J. Proc Natl Acad Sci U S A 1991, 88, 3569–3573.
55. Cao, W.; Lai, L. H. Biophys Chem 1999, 80, 217–226.
56. Jelesarov, I.; Crane-Robinson, C.; Privalov, P. L. J Mol Biol 1999, 294, 981–995.
57. Wu, P.; Sugimoto, N. Nucleic Acids Res 2000, 28, 4762–4768.
58. Dimitrov, R. A.; Zuker, M. Biophys J 2004, 87, 215–226.
59. Koehler, R. T.; Peyret, N. Bioinformatics 2005, 21, 3333–3339.
60. Mikulecky, P. J.; Feig, A. L. Biochemistry 2006, 45, 604–616.
61. Fang, X. W.; Golden, B. L.; Littrell, K.; Shelton, V.; Thiyagarajan, P.; Pan, T.; Sosnick, T. R. Proc Natl Acad Sci U S A 2001, 98, 4355–4360.
62. Takach, J. C.; Mikulecky, P. J.; Feig, A. L. J Am Chem Soc 2004, 126, 6530–6531.
63. Privalov, P. L. Crit Rev Biochem Mol Biol 1990, 25, 281–305.
64. Privalov, P. L.; Ptitsyn, O. B.; Birshtein, T. M. Biopolymers 1969, 8, 559–571.
65. Breslauer, K. J.; Frank, R.; Blocker, H.; Marky, L. A. Proc Natl Acad Sci U S A 1986, 83, 3746–3750.
66. Levy, J.; Biltonen, R. Biochemistry 1972, 11, 4145–4152.
67. Rouzina, I.; Bloomfield, V. A. Biophys J 1999, 77, 3242–3251.
68. Rouzina, I.; Bloomfield, V. A. Biophys J 1999, 77, 3252–3255.
69. Wu, P.; Nakano, S.; Sugimoto, N. Eur J Biochem 2002, 269, 2821–2830.
70. Tikhomirova, A.; Taulier, N.; Chalikian, T. V. J Am Chem Soc 2004, 126, 16387–16394.
71. Dubins, D. N.; Lee, A.; Macgregor, R. B., Jr.; Chalikian, T. V. J Am Chem Soc 2001, 123, 9254–9259.
72. Mikulecky, P. J.; Feig, A. L. J Am Chem Soc 2002, 124, 890–891.
73. Mikulecky, P. J.; Feig, A. L. Nucleic Acids Res 2004, 32, 3967–3976.
74. SantaLucia, J.; Turner, D. H. Biopolymers 1997, 44, 309–319.
75. Chalikian, T. V.; Volker, J.; Plum, G. E.; Breslauer, K. J. Proc Natl Acad Sci U S A 1999, 96, 7853–7858.
76. Diamond, J. M.; Turner, D. H.; Mathews, D. H. Biochemistry 2001, 40, 6971–6981.
77. Mathews, D. H.; Turner, D. H. Biochemistry 2002, 41, 869–880.
78. Mikulecky, P. J.; Takach, J. C.; Feig, A. L. Biochemistry 2004, 43, 5870–5881.
79. Petersheim, M.; Turner, D. H. Biochemistry 1983, 22, 256–263.
80. Albergo, D. D.; Marky, L. A.; Breslauer, K. J.; Turner, D. H. Biochemistry 1981, 20, 1409–1413.
81. Xia, T. B.; SantaLucia, J.; Burkard, M. E.; Kierzek, R.; Schroeder, S. J.; Jiao, X. Q.; Cox, C.; Turner, D. H. Biochemistry 1998, 37, 14719–14735.

82. Cooper, A.; Johnson, C. M. Methods Mol Biol 1994, 22, 137–150.
83. Cooper, A.; Johnson, C. M. Methods Mol Biol 1994, 22, 109–124.
84. Freire, E. Methods Mol Biol 1995, 40, 191–218.
85. Plum, G. E.; Breslauer, K. J. Curr Opin Struct Biol 1995, 5, 682–690.
86. Jelesarov, I.; Bosshard, H. R. J Mol Recognit 1999, 12, 3–18.
87. Privalov, P. L.; Plotnikov, V. V.; Filimonov, V. V. J Chem Thermodyn 1975, 7, 41–47.
88. Privalov, P. L.; Potekhin, S. A. Methods Enzymol 1986, 131, 4–51.
89. Sigurskjold, B. W. Anal Biochem 2000, 277, 260–266.
90. Naghibi, H.; Tamura, A.; Sturtevant, J. M. Proc Natl Acad Sci U S A 1995, 92, 5597–5599.
91. Liu, Y. F.; Sturtevant, J. M. Protein Sci 1995, 4, 2559–2561.
92. Chaires, J. B. Biophys Chem 1997, 64, 15–23.
93. Horn, J. R.; Russell, D.; Lewis, E. A.; Murphy, K. P. Biochemistry 2001, 40, 1774–1778.
94. Horn, J. R.; Brandts, J. F.; Murphy, K. P. Biochemistry 2002, 41, 7501–7507.
95. SantaLucia, J., Jr. Proc Natl Acad Sci U S A 1998, 95, 1460–1465.
96. Williams, M. C.; Wenner, J. R.; Rouzina, I.; Bloomfield, V. A. Biophys J 2001, 80, 1932–1939.
97. Scheffler, I. E.; Sturtevant, J. M. J Mol Biol 1969, 42, 577–580.
98. Marky, L. A.; Breslauer, K. J. Biopolymers 1982, 21, 2185–2194.
99. Bunville, L. G.; Geiduschek, E. P. Biopolymers 1965, 3, 213–240.
100. Sturtevant, J. M.; Rice, S. A.; Geiduschek, E. P. Discuss Faraday Soc 1958, 25, 138–149.
101. Klump, H.; Ackermann, T.; Neumann, E. Biopolymers 1969, 7, 423–431.
102. Breslauer, K. J.; Sturtevant, J. M.; Tinoco, I. J Mol Biol 1975, 99, 549–565.
103. Chipev, C. C.; Angelova, M. I. Int J Biol Macromol 1983, 5, 252–253.
104. Klostermeier, D.; Millar, D. P. Biochemistry 2000, 39, 12970–12978.
105. Brandts, J. F.; Jackson, W. M.; Ting, T. Y. Biochemistry 1974, 13, 3595–3600.
106. Bode, D.; Schernau, U.; Ackermann, T. Biophys Chem 1974, 1, 214–221.
107. Hinz, H. J.; Filimonov, V. V.; Privalov, P. L. Eur J Biochem 1977, 72, 79–86.
108. Rawitscher, M. A.; Ross, P. D.; Sturtevant, J. M. J Am Chem Soc 1963, 85, 1915–1918.
109. Neumann, E.; Ackermann, T. J Phys Chem 1967, 71, 2377–2379.
110. Krakauer, H.; Sturtevant, J. M. Biopolymers 1968, 6, 491–512.
111. Neumann, E.; Ackermann, T. J Phys Chem 1969, 73, 2170–2178.
112. Klump, H.; Ackermann, T. Biopolymers 1971, 10, 513–522.
113. Shiao, D. D. F.; Sturtevant, J. M. Biopolymers 1973, 12, 1829–1836.
114. Gruenwedel, D. W. Biochim Biophys Acta 1974, 340, 16–30.
115. Suurkuusk, J.; Alvarez, J.; Freire, E.; Biltonen, R. Biopolymers 1977, 16, 2641–2652.
116. Filimonov, V. V.; Privalov, P. L. J Mol Biol 1978, 122, 465–470.
117. Nordmeier, E. J Phys Chem 1992, 96, 1494–1501.
118. Korolev, N. I.; Vlasov, A. P.; Kuznetsov, I. A. Biopolymers 1994, 34, 1275–1290.
119. Freier, S. M.; Sugimoto, N.; Sinclair, A.; Alkema, D.; Neilson, T.; Kierzek, R.; Caruthers, M. H.; Turner, D. H. Biochemistry 1986, 25, 3214–3219.
120. Sugimoto, N.; Kierzek, R.; Freier, S. M.; Turner, D. H. Biochemistry 1986, 25, 5755–5759.
121. Park, Y. W.; Breslauer, K. J. Proc Natl Acad Sci U S A 1991, 88, 1551–1555.
122. Ross, P. D.; Howard, F. B.; Lewis, M. S. Biochemistry 1991, 30, 6269–6275.
123. Volker, J.; Makube, N.; Plum, G. E.; Klump, H. H.; Breslauer, K. J. Proc Natl Acad Sci U S A 2002, 99, 14700–14705.
124. Bourdelat-Parks, B. N.; Wartell, R. M. Biochemistry 2004, 43, 9918–9925.
125. Amrane, S.; Sacca, B.; Mills, M.; Chauhan, M.; Klump, H. H.; Mergny, J. L. Nucleic Acids Res 2005, 33, 4065–4077.
126. Howard, F. B.; Miles, H. T.; Ross, P. D. Biochemistry 1995, 34, 7135–7144.
127. Kamiya, M.; Torigoe, H.; Shindo, H.; Sarai, A. J Am Chem Soc 1996, 118, 4532–4538.
128. Asensio, J. L.; Dosanjh, H. S.; Jenkins, T. C.; Lane, A. N. Biochemistry 1998, 37, 15188–15198.
129. Torigoe, H.; Shimizume, R. Nucleic Acids Symp Ser 2000, 61–62.
130. Ross, P. D.; Howard, F. B. Biopolymers 2003, 68, 210–222.
131. Lu, M.; Guo, Q.; Marky, L. A.; Seeman, N. C.; Kallenbach, N. R. J Mol Biol 1992, 223, 781–789.
132. Ladbury, J. E.; Sturtevant, J. M.; Leontis, N. B. Biochemistry 1994, 33, 6828–6833.
133. Laing, L. G.; Draper, D. E. J Mol Biol 1994, 237, 560–576.
134. Hammann, C.; Cooper, A.; Lilley, D. M. Biochemistry 2001, 40, 1423–1429.
135. Levy, J.; Rialdi, G.; Biltonen, R. Biochemistry 1972, 11, 4138–4144.
136. Gluick, T. C.; Draper, D. E. J Mol Biol 1994, 241, 246–262.
137. Smirnov, I.; Shafer, R. H. Biochemistry 2000, 39, 1462–1468.

Reviewing Editor: Kenneth Breslauer